Received: 24 October 2025 | Revised: 1 December 2025 | Accepted: 19 December 2025

DOI: 10.1111/jace.70492

Journal of the American Ceramic Society

RESEARCH ARTICLE

Dislocation interaction with a tilt low-angle grain boundary in bi-crystal $SrTiO_3$

Kuan Ding[1] | **Atsutomo Nakamura**[2] | **Patrick Cordier**[3,4] | **Xufei Fang**[2,5]

[1]Department of Materials and Earth Sciences, Technical University of Darmstadt, Darmstadt, Germany

[2]Department of Mechanical Science and Bioengineering, The University of Osaka, Toyonaka, Japan

[3]Unité Matériaux et Transformations, Université de Lille, Villeneuve d'Ascq Cedex, France

[4]Institut universitaire de France (IUF), Paris, France

[5]Institute for Applied Materials, Karlsruhe Institute of Technology, Karlsruhe, Germany

Correspondence
Patrick Cordier, Unité Matériaux et Transformations, Université de Lille, 59655 Villeneuve-d'Ascq Cedex, France.
Email: patrick.cordier@univ-lille.fr

Xufei Fang, Institute for Applied Materials, Karlsruhe Institute of Technology, Karlsruhe, Germany.
Email: xufei.fang@kit.edu

Kuan Ding is currently at the Max Planck Institute for Sustainable Materials, Düsseldorf, Germany.

Xufei Fang was previously at the Department of Materials and Earth Sciences, Technical University of Darmstadt, Darmstadt, Germany.

Funding information
European Research Council, Grant/Award Numbers: 101076167, 787198

Abstract

For potentially wider applications of ceramics with dislocation-tuned mechanical and functional properties, it is pertinent to achieve dislocation engineering in polycrystalline ceramics. However, grain boundaries (GBs) in general are effective barriers for dislocation glide and often result in crack formation when plastic deformation in ceramics is attempted at room temperature. To develop strategies for crack suppression, it is critical to understand the fundamental processes for dislocation–GB interaction. For this purpose, we adopt a model system of bi-crystal $SrTiO_3$ with a 4° tilt GB, which consists of an array of edge dislocations. Room-temperature Brinell indentation was used to generate a plastic zone at the mesoscale without crack formation, allowing for direct assessment of GB-dislocation interaction in bulk samples. Together with dislocation etch pits imaging and transmission electron microscopy analysis, we observe dislocation pileup, storage, and transmission across the low-angle tilt GB. Our experimental observations reveal new insight into dislocation–GB interaction at room temperature at the mesoscale.

KEYWORDS
dislocation, low-angle tilt grain boundary, slip transmission, $SrTiO_3$, TEM

1 | INTRODUCTION

Dislocations in ceramics have been proven promising for tuning functional and mechanical properties.[1–10] To engineer dislocations into ceramic materials, mechanical deformation has been an effective way and is increasing attention, particularly at room temperature.[11] Dislocation-mediated plasticity has been proven feasible in bulk single-crystal oxides at either high temperature[4,7,12] or room temperature,[13–15] making single crystals an appealing

candidate for investigating dislocation-tuned functionality. However, polycrystalline ceramics are commonly used in applications, with much more cost-effective processing and fabrication than those of single crystals. Therefore, mechanical tailoring of dislocations in polycrystalline materials holds great potential for extending dislocation-tuned functionality into real applications.

Grain boundaries (GBs) in polycrystalline materials generally act as effective barriers for dislocation motion. Particularly for ceramics, the insufficient independent slip systems at room temperature[16] do not fulfill the von Mises or Taylor criterion which requires five independent slip systems for arbitrary plastic deformation,[17] making it challenging to engineer dislocations without crack formation using the mechanical deformation approach at the macroscale. For instance, tensile testing of polycrystalline MgO at room temperature showed that dislocations were initiated in the vicinity of the GBs, but no slip transmission across the GBs was observed.[18] Four-point bending tests of polycrystalline LiF showed that GBs were strong barriers to dislocation slip.[19] Bulk compression test of NaCl polycrystals at room temperature unveiled that low-angle GB (LAGB) allowed transmission of gliding dislocations, whereas high-angle GB (HAGB) acted as an impenetrable obstacle to gliding dislocations.[20] These earlier studies provided valuable insights into dislocation–GB interaction as well as crack formation during bulk deformation, yet the dislocation microstructures were not characterized due to the lack of advanced characterization techniques back then.

In order to gain a more detailed understanding of the interaction between dislocations and specific grain boundaries, recent studies have been carried out at the nanoscale in bi-crystal oxide ceramics. Kondo et al.[21] performed in situ nanoindentation in a TEM (transmission electron microscope) and directly observed the interaction of individual dislocations with a 1.2° tilt LAGB as well as a Σ5 HAGB in bi-crystal $SrTiO_3$. The processes with dislocations first impeded and then transmitted through this LAGB were visualized for the first time. In stark contrast, dislocation pileup and no transmission were found at the Σ5 HAGB. In a recent study, the same group led by Ikuhara observed dislocation transmission in twist LAGB as well as jog formation caused by the interaction between the grain boundary screw dislocations (as fabricated) and the incoming dislocations (induced by mechanical loading).[22] These in situ studies have advanced our understanding of the dislocation–GB interaction at the microscopic scale. However, to observe the dislocation structures in TEM, a thin foil with hundreds of nanometers must be used, resulting in different deformation boundary conditions and stress states than those in the bulk. The question remains as to what extent the deformation mechanisms obtained from in situ TEM deformation could be directly transferred or correlated with bulk deformation mechanisms.[23] In another study, Nakamura et al.[24] adopted bulk bi-crystals and investigated the nanoindentation response of ZrO_2 with different types of high-angle symmetrical tilt boundaries and $SrTiO_3$ with a symmetrical Σ5 boundary. They showed dislocation pileup, penetration, or generation through GBs by TEM characterization. Although the tests were carried out in bulk samples, the nanoindentation tests were limited to nano-/microscale. The size effects, as well as the high degree of local confinement in nanoindentation tests, limit this approach to represent the plastic deformation behavior at meso/macroscales.

To fill the gap in the length scale, Okafor et al.[25] recently adopted cyclic Brinell indentation with a millimeter-sized spherical indenter and achieved up to a dislocation density of $\sim 10^{13}$ m^{-2} in crack-free plastic zones with hundreds of micrometers in single-crystal $SrTiO_3$ at room temperature. This approach is simple and straightforward and allows the study of dislocation–GB interaction at the mesoscale up to the bulk scale which is relevant for functional and mechanical testing. Later, Okafor et al.[26] applied this method to polycrystalline coarse-grained $SrTiO_3$ and achieved near-surface plastic deformation without crack formation. They made use of the samples' free surface to relax the von Mises or Taylor criterion. However, a detailed dislocation–GB interaction at the mesoscale was not attempted.[26] Here, we adopt the Brinell indentation method[25] to engineer dislocations and make them interact with GB, using a bi-crystal $SrTiO_3$ sample containing a 4° tilt LAGB. The dislocation–GB interaction was first revealed at the surface by dislocation etch pit analysis. Furthermore, we perform TEM investigations of these specimens to gain a more in-depth understanding of the dislocation–GB interaction beneath the surface. Here, the choice of LAGB is made for simplicity in analyzing the dislocation structures as well as for establishing the Brinell indentation testing protocol on bi-crystal oxide. Further studies on high-angle grain boundaries, which can be more relevant for sintered polycrystalline samples, will be undertaken in the near future.

2 | MATERIALS AND METHODS

2.1 | Bi-crystal fabrication

The $SrTiO_3$ (STO) bi-crystal with a [001]/(110) 4° tilt grain boundary (Figure 1A,B) was fabricated using the thermal diffusion bonding technique.[27] Two STO single crystals with 2° off (110) surfaces were polished to mirror-like surfaces. Afterwards, the surfaces were cleaned with ethanol, and the two single crystals were attached to

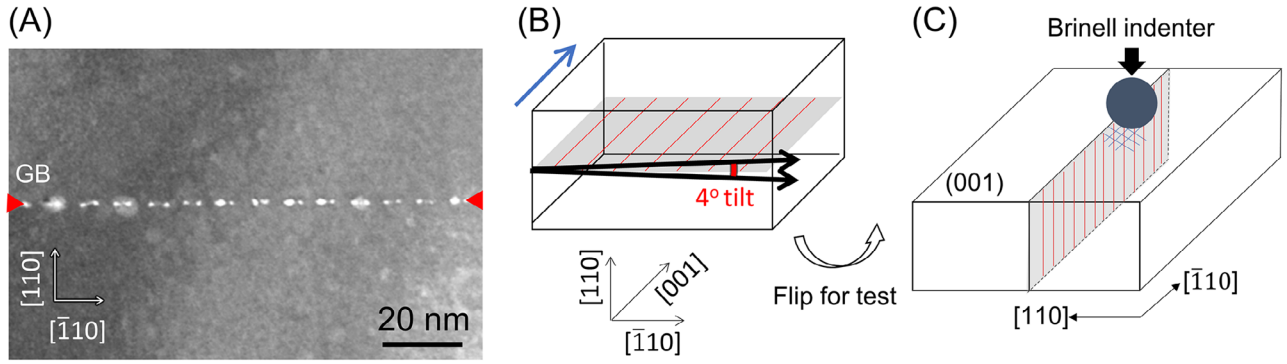

FIGURE 1 (A) Bright-field TEM image of the as-fabricated 4° tilt low-angle grain boundary (GB, as indicated by the red triangles). (B) Schematic of the bi-crystal fabrication and crystal orientation, with the GB plane (110) highlighted in grey, and the edge dislocations as red lines. (C) Schematic illustration of the Brinell indentation tests in one grain to induce dislocations without crack formation, allowing for dislocation–GB interaction studies. The patched lines underneath the indenter indicate the generated slip traces.

form a 4° tilt grain boundary, with the two crystals having a +2° and −2° inclination from the (110) surface around the [001] direction. The bi-crystal used in this study was prepared using the same conditions but with a different LAGB than in a study by Furushima et al.,[28] namely, by diffusion bonding at 1000°C for 10 h under a uniaxial load of 10 N. Further annealing at 1500°C in air for 10 h was performed to achieve sufficient atomic diffusion.

2.2 | Sample surface preparation

The sample surface (perpendicular to the GB plane, see Figure 1C) was metallographically prepared to obtain a smooth surface without inducing additional surface dislocations. The surface was mechanically ground using SiC-based grinding papers with grades from P1200 to P4000. The sample was then mechanically polished with diamond particles with sizes of 6, 3, 1, and 0.25 μm, respectively. The final polishing was carried out with colloidal silica polishing suspension OP-S (Struers, Germany) for ca. 15 h. Afterwards, the sample surface was cleaned with distilled water and then dried with ethanol.

2.3 | Brinell indentation

Brinell indentation tests[25] were performed using a universal hardness testing machine (Karl-Frank GmbH, Germany) mounted with a spherical indenter (hardened steel) with a diameter of 2.5 mm. A test load of 1.5 kg was used to generate dislocations without crack formation, allowing for direct investigation of the dislocation–GB interaction (Figure 1C).

2.4 | Microstructural characterization

Optical images of the sample surface after indentation were captured using a Zeiss Axio Imager 2 optical microscope (Zeiss, Germany) with circular differential interference contrast (C-DIC) and dark field mode. Dislocation etch pits study was carried out using chemical etching by immersing the sample in 50% HNO_3 containing 16 drops of HF solution for 50–60 s. The etched sample surface was characterized using a LEXT OLS4100 laser confocal microscope (Olympus, Japan). A thin layer of carbon was sputtered onto the sample surface before SEM characterization to reduce the surface charging. The SEM micrographs were taken in a Tescan MIRA 3 XMH SEM (Tescan, Czech Republic) with an accelerating voltage of 5 kV.

2.5 | TEM characterization

Before deformation, the as-fabricated grain boundary was examined (Figure 1A) using TEM. Before deformation, thin foils for TEM observation were prepared from the above-fabricated 4°-tilt low-angle grain boundary. The samples were initially sliced to include the grain boundary plane, followed by Ar^+ ion milling to achieve electron transparency. Dislocation arrays along the grain boundary were then examined using an ultra-high-voltage transmission electron microscope (JEOL JEM-1000k RS) operated at 1000 kV. After deformation, TEM characterizations were carried out using the electron microscopy facility of the Advanced Characterization Platform of the Chevreul Institute (University of Lille), with a FEI Tecnai G220Twin microscope, operating at 200 kV equipped with a LaB_6 filament. The TEM thin sections were prepared by focused ion beam (FIB) with a FIB/SEM ZEISS Crossbeam 550.

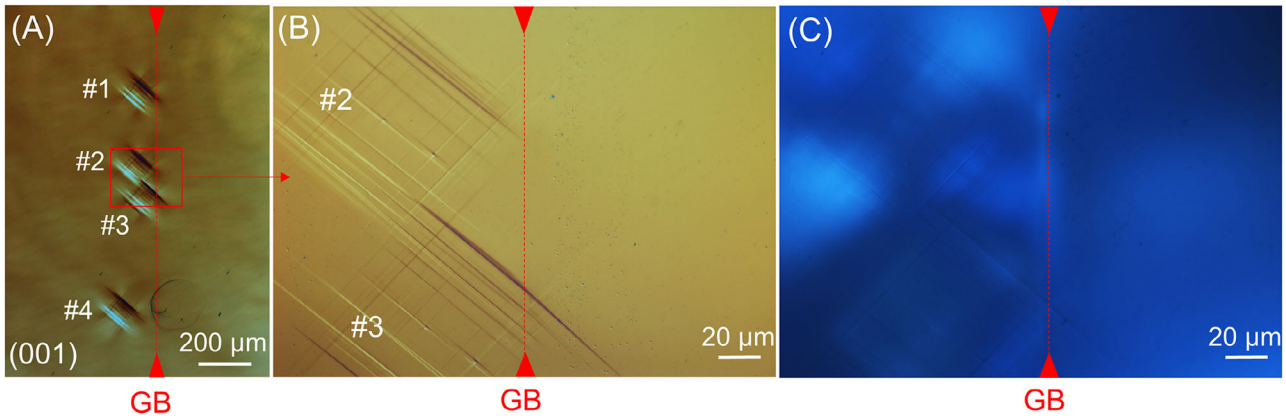

FIGURE 2 Optical images of representative Brinell indents near the grain boundary (GB). (A) Multiple indents were performed with different distances to the GB for optimizing the experimental parameters. (B) Zoom-in region showcasing the slip traces terminate (#2) or penetrate (#3) the GB. (C) Corresponding dark-field image of the region in (B), revealing no crack formation at the GB.

3 | RESULTS AND ANALYSES

As illustrated in the optical images in Figure 2, large plastic zones (~200 μm in diameter for the indent imprint) without crack formation have been achieved using Brinell indentation. This mesoscale approach is verified to be feasible, as multiple indents were performed at different distances from the GB for optimizing the testing conditions, giving excellent reproducibility in the plastic zones without crack formation. In particular, the distances of the indents to the GB were optimized to make sure that the new slip traces on the other side of the GB are not directly induced by the Brinell indenter itself. Here in Figure 2B, two indent imprints are highlighted, with the corresponding dark-field images (Figure 2C) corroborating no visible crack formation along the GB. Slip bands are observed that terminate on (#2 in Figure 2B) or transmit (#3 in Figure 2B) across the LAGB.

After optical image examination, the (001) surfaces were chemically etched to reveal the dislocation etch pits (Figure 3). The etched GB is identified as the vertical straight line across the sample surface (Figure 3A, yellow triangles). The Brinell indent was imprinted next to the GB on the right-side grain, with a load of 1.5 kg and 30 cycles. The higher number of cycles is used for this indent to generate sufficient dislocations to reach and penetrate the GB. The dense etch pits on the right side of the GB in Figure 3A correspond to dislocations generated within the Brinell imprint.

As revealed by the surface etch pits (Figure 3A), this 4° tilt LAGB can already effectively impede most of the dislocations. Several slip bands in the $[0\bar{1}0]$ and $[\bar{1}00]$ directions successfully transmitted (indicated by the white arrows in Figure 3A) across the grain boundary into the adjacent grain. Two of these transmission sites are highlighted in Figure 3B1,C1. To obtain the in-depth information on the dislocations–GB interactions at these two selected sites, TEM lamella lift-outs (Figure B2,C2) were performed parallel to the (010) planes. Note the yellow lines in Figure B1,C1 indicate the intersection of the (010) planes with the sample surface (001). The overview of the two TEM lamellae is shown in Figures S1 and S2.

For the first selected slip transmission site (Figure 3B), the GB region has been successfully captured in the TEM analysis, as indicated by the yellow triangles in Figure 4. The black stripe on the right of the GB is the thick sample region retained during FIB milling (see also the overview in Figure S1) to support the thin TEM lamella to minimize bending. In these dark-field TEM images, the dislocation lines are visualized by the bright line contrasts beneath the sample surface. The surface etch pits (green arrows) are successfully captured in Figure 4, with each etch pit tailed by a dislocation. These dislocations are in contrast with **g**: 002 (Figure 4) and 011 (Figure S3) and out of contrast with **g**: $01\bar{1}$ (Figure S4). They exhibit short segments compatible with inclusion in a plane inclined at 45° to the thin section. We therefore identify these dislocations as [011] dislocations gliding in $(01\bar{1})$. Figure S3 even shows that these dislocations are mostly oriented as screw dislocations, in agreement with the previous dislocation etch pit analysis by Javaid et al.[29] using nanoindentation tests. On the left grain, etch pits tailed by dislocations (yellow arrows at the surface) were also captured, corresponding to the transmitted dislocations as shown in Figure 3B1, which are shown here to belong to the $[011](01\bar{1})$ slip system. This observation directly supports the validity of the etch pit method for dislocation observation in $SrTiO_3$. Beneath the

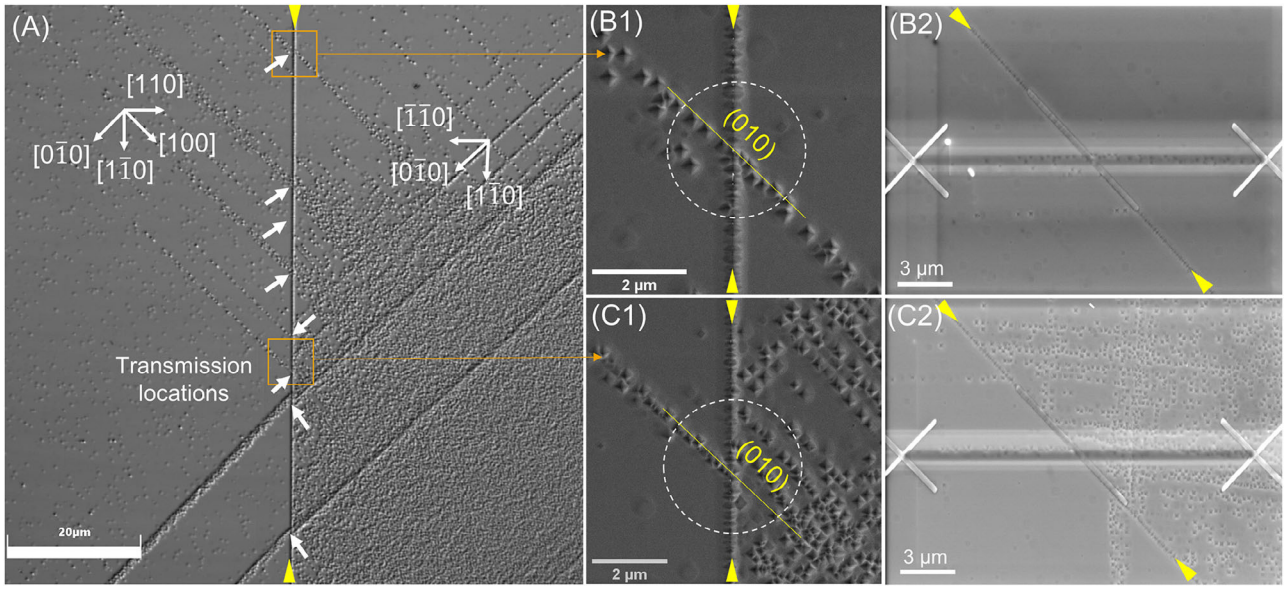

FIGURE 3 (A) Laser microscope image of dislocation–GB interaction from a Brinell indentation imprint (on the right grain) after chemical etching. The slip transmission sites are indicated by the white arrows. (B1, B2) SEM micrographs for the zoomed-in region for one slip transmission event. The X-X indicates the corresponding TEM lamella lift-out position for the same location, as B2 is 45° rotated with respect to B1; (C1, C2) SEM micrographs for the zoomed-in region for another slip transmission event. The X-X indicates the corresponding TEM lamella lift-out for in-depth observation, with C2 45° rotated with respect to C1. The GB is indicated by the yellow triangles in all cases.

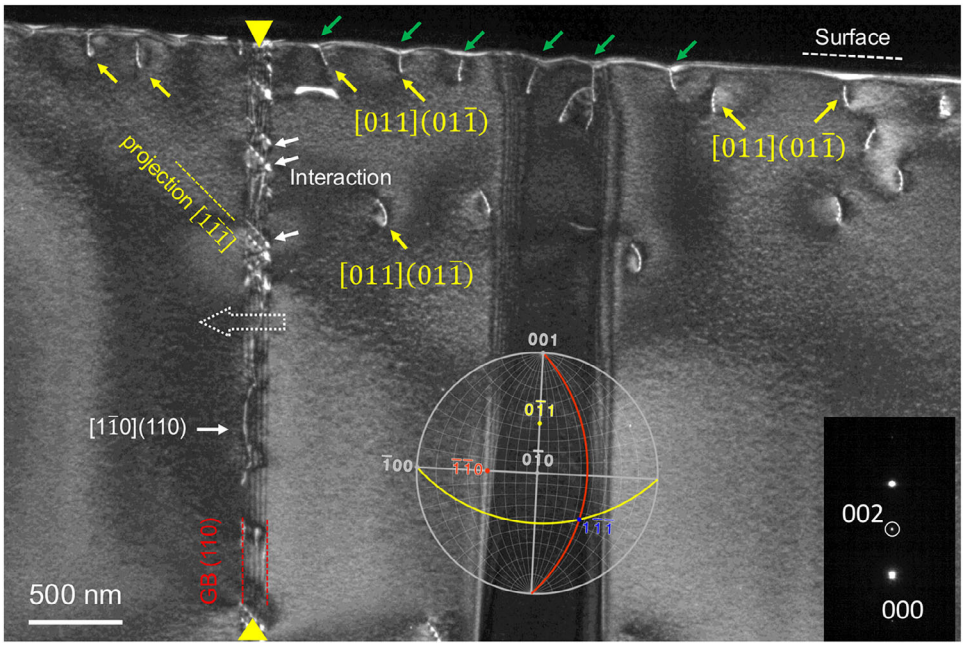

FIGURE 4 Weak-beam dark-field (g/2 g with g: 002) TEM observation of location 1 in Figure 3B. Overview of the dislocation–GB interaction with dislocations intersecting the free surface as well as the GB (thick yellow triangles).

surface, there are more dislocation lines observed (dislocation density higher than ~10^{12} m^{-2}), suggesting that the total dislocation density in the deformed region should be higher than merely counting the surface dislocation etch pits. Trapped dislocations are also present in the interface. The most frequent ones (marked in white) have orientations compatible with [1$\bar{1}\bar{1}$]. This was verified by observing the specimen under different orientations, close to the [0$\bar{1}$1] (Figure S3) and [0$\bar{1}\bar{1}$] (Figure S4) zone axes. Even though in one case (Figure S4) the dislocations are out of

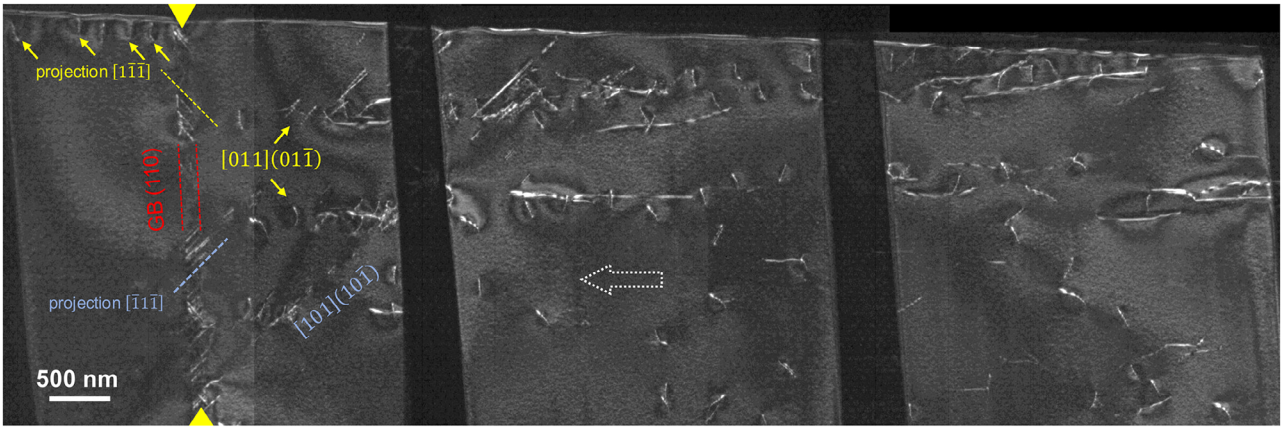

FIGURE 5 TEM lamella No. 2. Weak-beam dark-field (g/2 g with **g**: 200) TEM mosaic micrographs showing the dislocation microstructure below the surface. The LAGB location is highlighted by the yellow arrows on the left. The white dashed arrow indicates the travel direction of the dislocations induced by the Brinell indentation. More dislocations are observed to interact with the GB, leading to two distinct directions of lines of entrapped dislocations.

contrast, the orientations of the lines are compatible with the [1$\bar{1}\bar{1}$] direction, which is at the intersection between the LAGB (110) plane and that of the [011] dislocations: (01$\bar{1}$). Therefore, we interpret these lines as [011] dislocations trapped in the grain boundary interface. It should be noted that the LAGB shows other contrasts of dislocations. One of these is tentatively indicated by [1$\bar{1}$0](110) in Figure 4, although it has not been fully characterized. These marginal observations will not be discussed further.

Figures 5 and 6 present a second TEM thin section, which was FIB-milled from the interaction site shown in Figure 3C. The white dashed arrow in Figure 5 indicates the direction in which the dislocations travel. Here, we observe more dislocations generated on the right grain next to the GB (Figure 5). Transmitted dislocations across the GB are also observed at the surface (yellow arrows in Figure 5). Some dislocations in the right grain have all the characteristics of those analyzed in Figure 4 and Figures S3 and S4. We therefore identify them as [011](01$\bar{1}$) dislocations (marked in yellow). This identification is further supported here by the fact that they are in contrast with **g**: 200 (Figure S5). Another family of dislocations (marked in blue) is in contrast with **g**: 011 (Figure S6), 200 (Figures 5 and 6; Figure S5), and 002 (Figures 6 and 7). They are also contained in the (10$\bar{1}$) plane, which is edge-on in Figure 6. Therefore, we interpret these dislocations as belonging to the [101](10$\bar{1}$) slip system. These dislocations give rise to another family of lines trapped in the interface with a different orientation from that of the [011](01$\bar{1}$) dislocations. Observation of the specimen near the zone axes [010] (Figures 5 and 6), [0$\bar{1}\bar{1}$] (Figure S5), and [0$\bar{1}$1] (Figure S6) allows the direction of these lines to be identified as [$\bar{1}$1$\bar{1}$], which is indeed the intersection between the (110) and (10$\bar{1}$) planes. Furthermore, Figure 7 demonstrates that both [011](01$\bar{1}$) and [101](10$\bar{1}$) dislocations are eventually transmitted across the LAGB into the left grain.

4 | DISCUSSION

4.1 | Dislocation–GB interaction

The results above confirm that the dislocation transmission behavior in low-angle tilt GB in STO, as previously visualized directly at the nanoscale via in situ TEM by Kondo et al.,[21] is transferable to a much larger scale, namely at the mesoscale/bulk, as in the current case, provided that crack formation can be suppressed.

The results in Figures 3–7 reveal complex dislocation–GB interaction processes even for a simple tilt LAGB. Besides dislocation pile-up and transmission, it appears that dislocation storage also occurs at the GB for both [011](01$\bar{1}$) and [101](10$\bar{1}$) slip systems activated. The common criteria to describe the feasibility for slip transmission is the m' factor[30]:$\boldsymbol{m'} = \cos\phi \cos\kappa$, where ϕ is the angle between the slip plane normal, and κ is the angle between the slip directions. The absolute value of m' is between 0 and 1, with m' being close to 1 for easy slip transmission. The calculated m' value for LAGB is 0.9976, suggesting slip transmission is easier to occur for the LAGB. The possible dislocation–GB interaction is illustrated in Figure 8. As illustrated in the experimental observation (Figures 4 and 5), it is evident that there is partly transmission of the dislocations but also partly dislocation reaction and/or dislocation storage in the LAGB. In what follows, we discuss these possible scenarios.

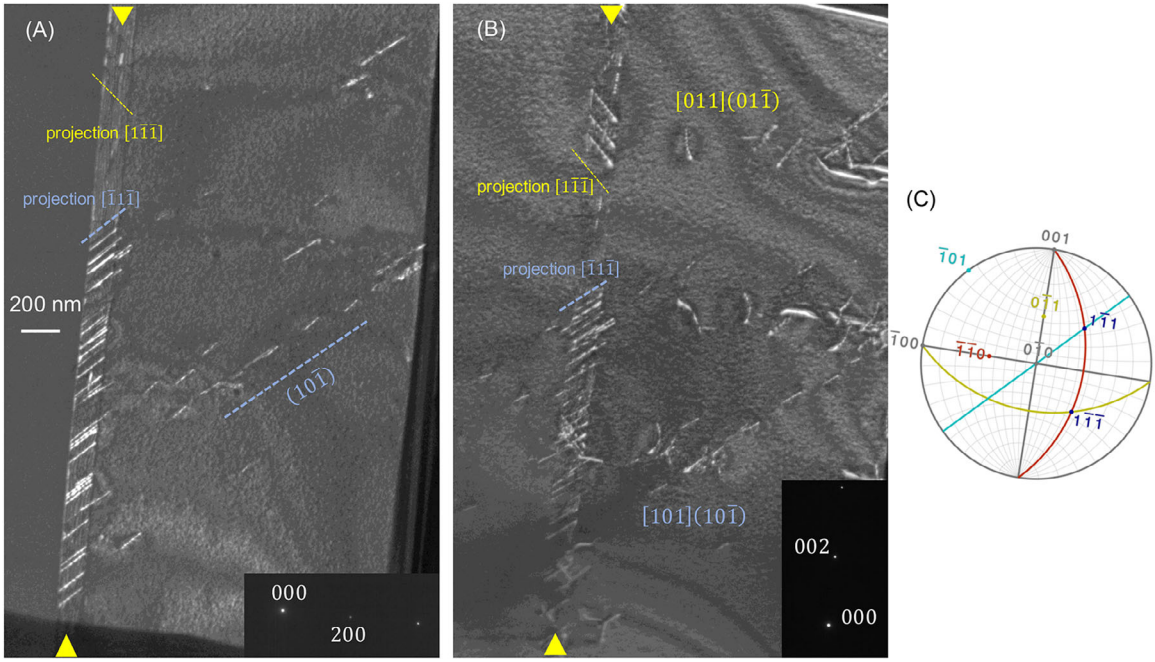

FIGURE 6 TEM lamella No. 2, with region near the LAGB showing dislocations heading toward it. (A) Weak-beam dark-field (g/2 g with **g**: 200) close to the [0$\bar{1}$0] zone axis (see stereoplot in subfigure C). (B) Weak-beam dark-field (g/2 g with **g**: 002) close to the [0$\bar{1}$0] zone axis. The line directions of dislocations entrapped in the LAGB are parallel to [1$\bar{1}\bar{1}$] (yellow) and [$\bar{1}$1$\bar{1}$] (blue). [011] dislocations (yellow) are out of contrast in (A). The glide plane of [101] dislocations (blue) is seen edge-on.

As illustrated in Figure 1, the LAGB has a plane of (110), and is made up of an array of edge dislocations with [1$\bar{1}$0] Burgers vector. It is likely that storage is a consequence of reactions between the GB dislocations and the incoming screw dislocations. In case of [011](01$\bar{1}$) incoming dislocations, the reaction [011] + [1$\bar{1}$0] = [101], is energetically favorable, inducing a tendency to storage. As for the dislocations [101](10$\bar{1}$), the reaction would be [101] + [1$\bar{1}$0] = [2$\bar{1}$1] which is not favorable according to Frank's energy criterion.[29] However, this analysis considers perfect dislocations instead of dissociated dislocations, with the latter being the case for STO at room temperature.[31,32] Consider the stacking fault energy of STO is high (~136 mJ/m^2 for room temperature[31]) and the partials are spread a few unit cells apart,[32,33] leading to more complex situations with extended nodes as illustrated in Besson et al.[34]. We expect future work with more detailed but strenuous characterization with advanced TEM to provide more detailed information to confirm dislocation reactions, preferably coupled with atomistic simulations, which is beyond the current scope of the work.

It is also worth noting that Kondo et al.[21] directly visualized transmission of screw dislocations across an LAGB (with the GB dislocations having a Burgers vector of [100], different from the current case) in bi-crystal STO in their in situ TEM indentation tests. The differences are also reflected in the transmitted dislocations, which exhibited a newly formed superjog segment with a Burgers vector of [1$\bar{1}$1] according to the reaction of $\mathbf{b}_{\text{Jog}} = \mathbf{b}_{\text{Lattice}} + \mathbf{b}_{\text{GB}}$ = [0$\bar{1}$1] + [100] = [1$\bar{1}$1]. Nevertheless, LAGBs in STO seem to allow for easy slip transmission regardless of their GB configuration.

As schematically indicated in Figure 8, the dislocations induced by Brinell indentation are predominantly screw types. This has been reported and confirmed elsewhere.[21,25,35,36] The slip planes activated are of {110} types; when projected on the TEM samples plane, 45° inclined dislocation line contrasts will be formed, as observed in Figures 4 and 5. In particular, 4 equivalent {110} planes can be activated, with a 45° inclined angle to the sample surface. This means that for TEM lamella 1 (in Figure 4), it is likely that only one of these 45° slip planes was activated, corresponding to the single slip trace and single array of dislocation etch pits in Figure 3B1. For TEM lamella 2 (Figure 5), the multiple, mutually perpendicular slip traces, as well as the arrays of dislocation etch pits, suggest more than one of such 45° slip planes has been activated. The projections along the TEM lamella, hence, will generate not only 45° but also 135° (or minus 45°) inclined dislocation lines with respect to the sample surface, as confirmed by the TEM observation in Figure 5A.

At the transmission site shown in Figure 3B1, the etch-pit arrays on both sides of the grain boundary (GB) exhibit a continuous slip band crossing the boundary. Consistently, the corresponding weak-beam dark-field (WBDF) images in Figure 4 reveal a continuous line of [011](01$\bar{1}$)

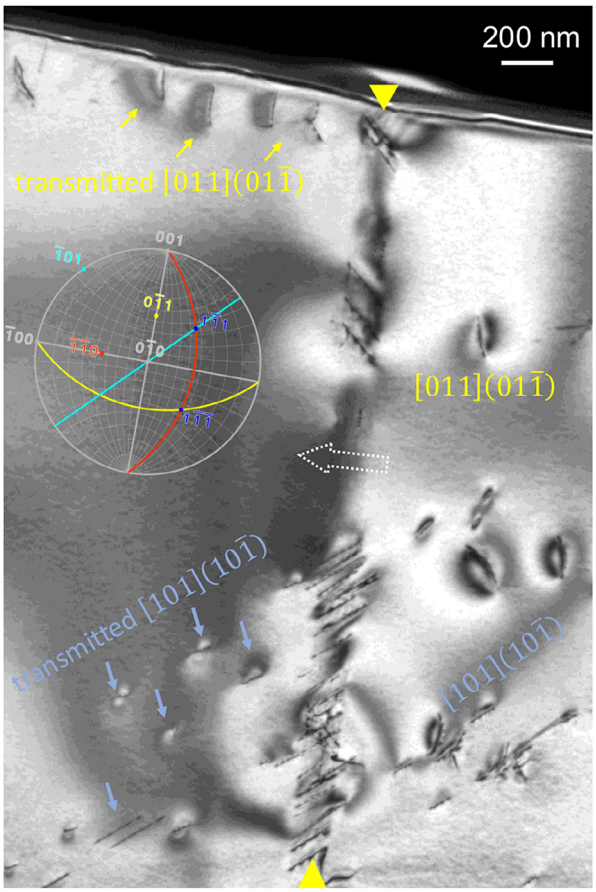

FIGURE 7 TEM lamella No. 2, with the same region as in Figure 6. Dark-field with **g**: 002 close to the [0$\bar{1}$0] zone axis. The diffraction conditions are adjusted to highlight dislocations on both sides of the LAGB. Both [011] and [101] dislocations are transmitted.

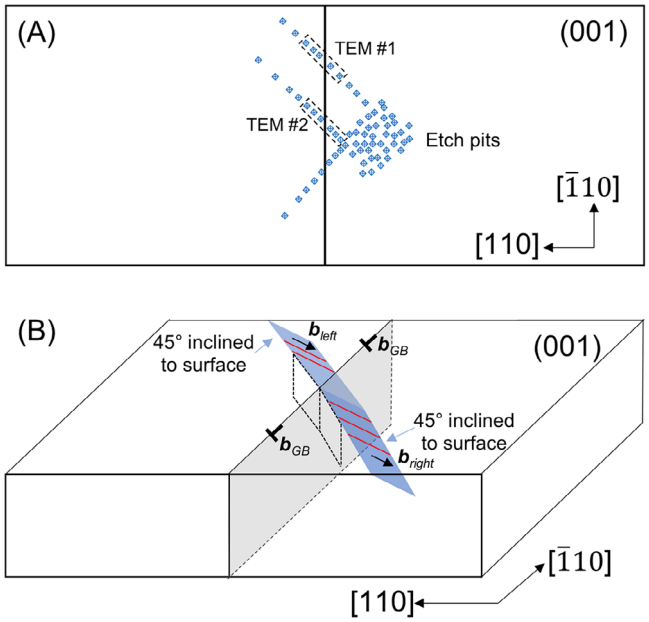

FIGURE 8 (A) 2D plan view of the indented area near GB, with the two TEM lamellae lift-outs indicated. The blue squares in the right grain indicate the dislocation etch pits, with the activated slip planes {110} being 45° inclined to the sample (001) surface. The dislocation lines, indicated in red, are predominantly screw types. (B) 3D perspective of a representative slip plane with dislocation transmission into the adjacent grain. These dislocation lines, when projected to the TEM lamellae planes (black dashed rhombus), will be 45° inclined.

dislocations traversing the GB, demonstrating a direct transmission event.[37] In contrast, the configuration in Figure 3C1 shows a finite offset of ~500 nm between the incoming dislocations on the right side of the GB and the outgoing array on the left side. This is corroborated by the TEM observation in Figure 5: [011](01$\bar{1}$) dislocations are observed on the left grain—consistent with the surface etch pits—whereas no corresponding dislocations are present at the surface on the right side. The absence of a geometric continuation across the GB rules out direct slip transmission at this location. Instead, a dense pileup of dislocations is observed on the right side of the GB, adjacent to the outgoing array. Such pileups can substantially elevate the local stress at the GB,[38] providing a sufficient driving force to activate {110}⟨011⟩ slip in the neighboring grain. The outgoing dislocation array is therefore most plausibly interpreted as newly nucleated from the GB acting as a dislocation source, rather than as the product of direct transmission.

The discussions based on Figure 8 raise questions on the applicability of conventional models using pure geometric mismatch-based slip transfer metrics in predicting the slip transfer in oxides, as these models are only formulated in terms of the misorientation angles by simply assuming a transmission can happen when $\theta < 15°$. The local atomistic structure at the slip-GB intersection, as well as the activated slip systems that are interacting with the GB, plays an important role in determining whether a transmission will occur or not. If the local structure, such as the one corresponding to a GB dislocation, carries the same Burgers vector as that of the incoming dislocation, it will introduce a strong repulsive force acting on the incoming dislocation. A pileup can still form due to such a strong repulsive force, even if the misorientation angle across the GB is as low as $\theta = 4°$. It should be noted that even though pileup of dislocations is observed at LAGB, the contribution of a single GB to the Hall–Petch strengthening in ceramics at room temperature is negligible.[24] Furthermore, the relatively higher Peierls barrier[39] and high stacking fault energy[31,40] lead to the low mobility of screw dislocations, resulting in a limited number of transmitted dislocations. Moreover, Kondo et al.[21] proposed that the lattice screw dislocations can react with the grain boundary edge dislocations to form jogs when crossing the LAGB. Using dark-field TEM imaging, they observed a shift in the GB edge dislocation

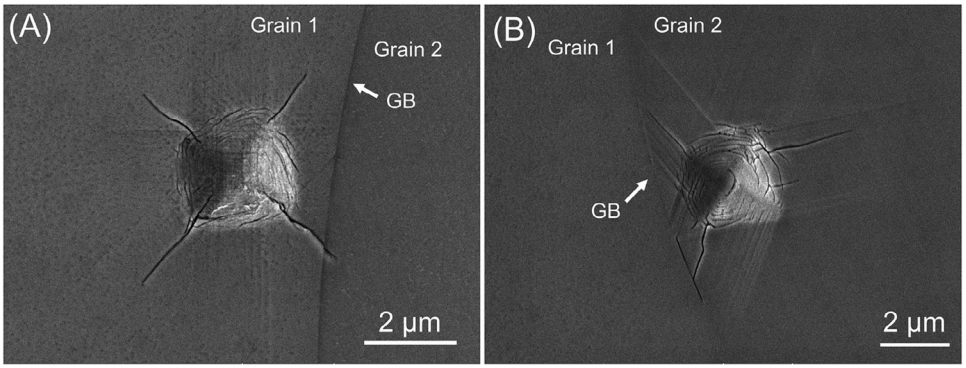

FIGURE 9 SEM micrographs of the indentation imprints left by using nanoindentation with an effective indenter tip radius of 2 μm at a maximum load of 75 mN. Both indent imprints reveal slip traces accompanied by crack formation, making the pure dislocation–GB interaction analysis challenging. Note that the sample was chemically etched to reveal the dislocation etch pits, and the tests were performed on a coarse-grained $SrTiO_3$ to allow for probing different GBs, two of which are showcased here in (A) and (B).

lines with super-jogs formed on the GB dislocations as well as kinks on the lattice dislocations. Trapped or stored lattice dislocations were also observed on the GB plane. This may well have altered the local atomic structure. However, a more detailed investigation of such local atomic structure changes requires high-resolution TEM (HRTEM) or HAADF (high-angle annular dark-field) imaging,[41,42] which is beyond the authors' capacity at the current stage.

4.2 | Crack suppression using Brinell indentation

A critical aspect to account for during room-temperature plastic deformation in ceramics is the cracking. Considering the size-dependent competition between cracking and plasticity in ceramics deformation, it is pertinent to illustrate more details on the choice of Brinell indentation for investigating dislocation–GB interaction. Even for $SrTiO_3$[13] and MgO[43], the two well-known oxides that exhibit excellent room-temperature dislocation plasticity in bulk deformation, crack formation can still be easily triggered. In the indentation case, due to the confinement and local hydrostatic compressive stress, dislocation plasticity is favored as in the case of Brinell indentation[15,25,26] (see also Figure 2). Nevertheless, a strong size-dependent competition between the dislocation plasticity and crack formation has been recently identified,[44] which concerns primarily the incipient plasticity as well as the crack formation due to the dislocation pile-up and dislocation interaction[45] underneath the indenter. To be specific, a smaller indenter may favor dislocation nucleation, yet cracks are also more easily formed due to the dislocation pileup and interaction that occurs more easily due to the much higher stress level and higher degree of dislocation multiplication. This is evidenced by, for example, a sharp Berkovich indenter[46] or spherical indentation with smaller indenter tips.[36] The formation of cracks, as well as the confined dislocation distribution induced by smaller indentation, results in complications for dislocation–GB interaction, as illustrated in Figure 9, where cracks may proceed before dislocation–GB interaction. In this regard, lowering the stress level by using a larger indenter is beneficial in crack suppression. This works for the oxides such as $SrTiO_3$, MgO, LiF, and many more ceramics[47] that exhibit good dislocation mobility at room temperature. This also merits the general applicability of the Brinell indentation and scratching approach for exploring dislocation–GB interactions at the mesoscale.

5 | CONCLUSION

Room-temperature Brinell indentation is adopted as a feasible approach to induce plastic zones up to hundreds of micrometers without crack formation in model perovskite oxide $SrTiO_3$, allowing for mesoscale assessment of dislocation–GB interactions in its bi-crystal. The combined near-surface analysis by dislocation etch pits study, as well as the in-depth information obtained by TEM analysis in the grain interior, reveals that 4° tilt LAGB, although being rather simple as an array of edge dislocations, exhibits a very complex dislocation–GB interaction, including trapping, storage, and slip transmission. This mesoscale indentation approach, when combined with the scratching test, allows for probing multiple and different types of grain boundaries, and can help to pave the road for high-throughput analysis of dislocation–GB interactions at meso-/macroscale.

ACKNOWLEDGMENTS

X. Fang acknowledges the financial support by the European Research Council (ERC-Starting Grant, Project MECERDIS, grant no. 101076167). P. Cordier is supported by the European Research Council (ERC) under the European Union's Horizon 2020 research and innovation program under grant agreement no. 787198 – TimeMan. FIB preparations are supported by the French RENATECH network, the CPER Hauts de France project IMITECH, and the Métropole Européenne de Lille. Views and opinions expressed are, however, those of the authors only and do not necessarily reflect those of the European Union or European Research Council. Neither the European Union nor the granting authority can be held responsible for them. We thank Prof. K. Durst and Prof. J. Rödel at TU Darmstadt for access to the laser microscope, SEM, and optical microscope, as well as Prof. W. Rheinheimer at the University of Stuttgart for providing the sample for us to perform the nanoindentation tests near the grain boundary.

Open access funding enabled and organized by Projekt DEAL.

CONFLICT OF INTEREST STATEMENT

The authors declare no conflict of interest.

ORCID

Kuan Ding https://orcid.org/0000-0003-0633-1954
Atsutomo Nakamura https://orcid.org/0000-0002-4324-1512
Patrick Cordier https://orcid.org/0000-0002-1883-2994

References

1. Nakamura A, Matsunaga K, Tohma J, Yamamoto T, Ikuhara Y. Conducting nanowires in insulating ceramics. Nat Mater. 2003;2(7):453–56. https://doi.org/10.1038/nmat920
2. Ikuhara Y. Nanowire design by dislocation technology. Prog Mater Sci. 2009;54(6):770–91. https://doi.org/10.1016/j.pmatsci.2009.03.001
3. Sun B, Haunschild G, Polanco C, Ju JZ, Lindsay L, Koblmuller G, et al. Dislocation-induced thermal transport anisotropy in single-crystal group-III nitride films. Nat Mater. 2019;18(2):136–40. https://doi.org/10.1038/s41563-018-0250-y
4. Höfling M, Zhou X, Riemer LM, Bruder E, Liu B, Zhou L, et al. Control of polarization in bulk ferroelectrics by mechanical dislocation imprint. Science. 2021;372:961–64. https://doi.org/10.1126/science.abe3810
5. Hameed S, Pelc D, Anderson ZW, Klein A, Spieker RJ, Yue L, et al. Enhanced superconductivity and ferroelectric quantum criticality in plastically deformed strontium titanate. Nat Mater. 2022;21:54–61. https://doi.org/10.1038/s41563-021-01102-3
6. Zhang H, Gao S, Wang H, Zhuo F, Muhammad QK, Fang X, et al. Enhancing the photoelectric performance of metal oxide semiconductors by introduction of dislocations. J Mater Chem A. 2024;12:23910–19. https://doi.org/10.1039/D4TA03786C
7. Muhammad QK, Porz L, Nakamura A, Matsunaga K, Rohnke M, Janek J, et al. Donor and acceptor-like self-doping by mechanically induced dislocations in bulk TiO_2. Nano Energy. 2021;85:105944. https://doi.org/10.1016/j.nanoen.2021.105944
8. Salem MN, Ding K, Rödel J, Fang X. Thermally enhanced dislocation density improves both hardness and fracture toughness in single-crystal $SrTiO_3$. J Am Ceram Soc. 2023;106:1344–55. https://doi.org/10.1111/jace.18839
9. Fang X, Nakamura A, Rödel J. Deform to perform: dislocation-tuned properties of ceramics. ACerS Bulletin. 2023;102(5):24–29.
10. Fang X, Lu W, Zhang J, Minnert C, Hou J, Bruns S, et al. Harvesting room-temperature plasticity in ceramics by mechanically seeded dislocations. Mater Today. 2025;82:81–91. https://doi.org/10.1016/j.mattod.2024.11.014
11. Fang X. Mechanical tailoring of dislocations in ceramics at room temperature: a perspective. J Am Ceram Soc. 2024;107(3):1425–47. https://doi.org/10.1111/jace.19362
12. Nakamura A, Lagerlöf KPD, Matsunaga K, Tohma J, Yamamoto T, Ikuhara Y. Control of dislocation configuration in sapphire. Acta Mater. 2005;53(2):455–62. https://doi.org/10.1016/j.actamat.2004.10.002
13. Brunner D, Taeri-Baghbadrani S, Sigle W, Rühle M. Surprising results of a study on the plasticity in strontium titanate. J Am Ceram Soc. 2001;84(5):1161–63. https://doi.org/10.1111/j.1151-2916.2001.tb00805.x
14. Mark AF, Castillo-Rodriguez M, Sigle W. Unexpected plasticity of potassium niobate during compression between room temperature and 900°C. J Eur Ceram Soc. 2016;36(11):2781–93. https://doi.org/10.1016/j.jeurceramsoc.2016.04.032
15. Fang X, Zhang J, Frisch A, Preuß O, Okafor C, Setvin M, et al. Room-temperature bulk plasticity and tunable dislocation densities in $KTaO_3$. J Am Ceram Soc. 2024;107:7054–61. https://doi.org/10.1111/jace.20040
16. Anderson PM, Hirth JP, Lothe J. Theory of dislocations, 3rd ed., Cambridge University Press, 2017.
17. Groves GW, Kelly A. Independent slip systems in crystals. Philos Mag. 1963;8(89):877–87. https://doi.org/10.1080/14786436308213843
18. Sinha MN, Lloyd DJ, Tangri K. Microyield and fracture in polycrystalline MgO. J Mater Sci. 1973;8:116–22. https://doi.org/10.1007/BF00755590
19. Scott WD, Pask JA. Deformation and fracture of polycrystalline lithium fluoride. J Am Ceram Soc. 1963;46(6):284–93. https://doi.org/10.1111/j.1151-2916.1963.tb11728.x
20. Nadgornyi EM, Strunk HP. Dislocation structure of plastically deformed NaCl polycrystals. Physica Status Solidi (a). 1987;104(1):193–202 https://doi.org/10.1002/pssa.2211040114
21. Kondo S, Mitsuma T, Shibata N, Ikuhara Y. Direct observation of individual dislocation interaction processes with grain boundary. Sci Adv. 2016;2:e1501926. https://doi.org/10.1126/sciadv.1501926
22. Kondo S, Shibata N, Ikuhara Y. Direct observations of jog formation and drag caused by screw-screw dislocation interaction. Scr Mater. 2025;258:116513. https://doi.org/10.1016/j.scriptamat.2024.116513
23. Legros M, Mompiou F, Caillard D. Observing deformation in situ. Nat Mater. 2024;23(1):20–22. https://doi.org/10.1038/s41563-023-01739-2

24. Nakamura R, Masuda H, Yoshida H. Nanoindentation responses near single grain boundaries in oxide ceramics. J Am Ceram Soc. 2022;106(3):2061–72. https://doi.org/10.1111/jace.18887
25. Okafor C, Ding K, Zhou X, Durst K, Rödel J, Fang X. Mechanical tailoring of dislocation densities in $SrTiO_3$ at room temperature. J Am Ceram Soc. 2022;105:2399–402. https://doi.org/10.1111/jace.18277
26. Okafor C, Ding K, Preuß O, Khansur N, Rheinheimer W, Fang X. Near-surface plastic deformation in polycrystalline $SrTiO_3$ via room-temperature cyclic Brinell indentation. J Am Ceram Soc. 2024;107:6715–28. https://doi.org/10.1111/jace.19962
27. Ikuhara Y, Nishimura H, Nakamura A, Matsunaga K, Yamamoto T, Lagerloef KPD. Dislocation structures of low-angle and near-sigma 3 grain boundaries in alumina bicrystals. J Am Ceram Soc. 2003;86(4):595–602. https://doi.org/10.1111/j.1151-2916.2003.tb03346.x
28. Furushima Y, Arakawa Y, Nakamura A, Tochigi E, Matsunaga K. Nonstoichiometric [012]dislocation in strontium titanate. Acta Mater. 2017;135:103–11. https://doi.org/10.1016/j.actamat.2017.06.017
29. Javaid F, Johanns KE, Patterson EA, Durst K. Temperature dependence of indentation size effect, dislocation pile-ups, and lattice friction in (001) strontium titanate. J Am Ceram Soc. 2018;101(1):356–64. https://doi.org/10.1111/jace.15182
30. Javaid F, Pouriayevali H, Durst K. Dislocation–grain boundary interactions: recent advances on the underlying mechanisms studied via nanoindentation testing. J Mater Res. 2021;36(12):2545–57. https://doi.org/10.1557/s43578-020-00096-z
31. Matsunaga T, Saka H. Transmission electron microscopy of dislocations in $SrTiO_3$. Philos Mag Lett. 2000;80(9):597–604. https://doi.org/10.1080/09500830050134309
32. Porz L, Klomp AJ, Fang X, Li N, Yildirim C, Detlefs C, et al. Dislocation-toughened ceramics. Materials Horizons. 2021;8:1528–37. https://doi.org/10.1039/D0MH02033H
33. Zhang J, Fang X, Lu W. Impact of dislocation densities on the microscale strength of single-crystal strontium titanate. Acta Mater. 2025;291:121004. https://doi.org/10.1016/j.actamat.2025.121004
34. Besson P, Poirier JP, Price GD, Dislocations in $CaTiO_3$ perovskite deformed at high–temperature: a transmission electron microscopy study. Phys Chem Minerals. 1996;23:337334. https://doi.org/10.1007/BF00199499
35. Javaid F, Stukowski A, Durst K. 3D Dislocation structure evolution in strontium titanate: spherical indentation experiments and MD simulations. J Am Ceram Soc. 2017;100(3):1134–45. https://doi.org/10.1111/jace.14626
36. Fang X, Ding K, Minnert C, Nakamura A, Durst K. Dislocation-based crack initiation and propagation in single-crystal $SrTiO_3$. J Mater Sci. 2021;56:5479–92. https://doi.org/10.1007/s10853-020-05587-2
37. Nieto-Valeiras E, Orozco-Caballero A, Sarebanzadeh M, Sun J, Llorca J. Analysis of slip transfer across grain boundaries in Ti via diffraction contrast tomography and high-resolution digital image correlation: when the geometrical criteria are not sufficient. Int J Plast. 2024;175:103941. https://doi.org/10.1016/j.ijplas.2024.103941
38. Guo Y, Britton TB, Wilkinson AJ. Slip band–grain boundary interactions in commercial-purity titanium. Acta Mater. 2014;76:1–12. https://doi.org/10.1016/j.actamat.2014.05.015
39. Li Y, Liu X, Zhang P, Han Y, Huang M, Wan C. Theoretical insights into the Peierls plasticity in $SrTiO_3$ ceramics via dislocation remodelling. Nat Commun. 2022;13(1):6925. https://doi.org/10.1038/s41467-022-34741-4
40. Castillo-Rodríguez M, Sigle W. Dislocation dissociation and stacking-fault energy calculation in strontium titanate. Scr Mater. 2010;62(5):270–73. https://doi.org/10.1016/j.scriptamat.2009.11.016
41. Wei J, Feng B, Tochigi E, Shibata N, Ikuhara Y. Direct imaging of the disconnection climb mediated point defects absorption by a grain boundary. Nat Commun. 2022;13(1):1455. https://doi.org/10.1038/s41467-022-29162-2
42. Wei J, Feng B, Ishikawa R, Yokoi T, Matsunaga K, Shibata N, et al. Direct imaging of atomistic grain boundary migration. Nat Mater. 2021;20:951955. https://doi.org/10.1038/s41563-020-00879-z
43. Stokes RJ, Johnston TL, Li CH. Crack formation in magnesium oxide single crystals. Philos Mag. 1958;3(31):718–25. https://doi.org/10.1080/14786435808237008
44. Fang X, Bishara H, Ding K, Tsybenko H, Porz L, Höfling M, et al. Nanoindentation pop-in in oxides at room temperature: dislocation activation or crack formation?, J Am Ceram Soc. 2021;104:4728–41. https://doi.org/10.1111/jace.17806
45. Keh AS, Li JCM, Chou YT. Cracks due to the pilling-up of dislocations on two intersecting slip planes in MgO crystals. Acta Metall. 1959;7:694–96. https://doi.org/10.1016/0001-6160(59)90156-7
46. Javaid F, Bruder E, Durst K. Indentation size effect and dislocation structure evolution in (001) oriented $SrTiO_3$ Berkovich indentations: HR-EBSD and etch-pit analysis. Acta Mater. 2017;139:1–10. https://doi.org/10.1016/j.actamat.2017.07.055
47. Frisch A, Okafor C, Preuß O, Zhang J, Matsunaga K, Nakamura A, et al. Room-temperature dislocation plasticity in ceramics: methods, materials, and mechanisms. J Am Ceram Soc. 2025;108:e20575. https://doi.org/10.1111/jace.20575

SUPPORTING INFORMATION

Additional supporting information can be found online in the Supporting Information section at the end of this article.

How to cite this article: Ding K, Nakamura A, Cordier P, Fang X. Dislocation interaction with a tilt low-angle grain boundary in bi-crystal $SrTiO_3$. J Am Ceram Soc. 2026;109:e70492. https://doi.org/10.1111/jace.70492